Electronic Supplementary Information

for

Low-overpotential CO_2 reduction by phosphine-substituted Ru(II) polypyridyl complex

Sze Koon Lee,[a,b] Mio Kondo,[a,b,c] Go Nakamura,[a,b] Masaya Okamura,[a,d]
Shigeyuki Masaoka*[a,b]

[a]*Institute for Molecular Science (IMS), 5-1 Higashiyama, Myodaiji, Okazaki, Aichi 444-8787, Japan*.
[b]*Department of Structural Molecular Sciences, SOKENDAI (The Graduate University for Advanced Studies), Shonan village, Hayama, Kanagawa 240-0193, Japan*.
[c]*ACT-C, Japan Science and Technology Agency (JST), 4-1-8 Honcho, Kawaguchi, Saitama 332-0012, Japan*.
[d]*Graduate School of Science, Nagoya University, Furo-cho, Chikusa-ku, Nagoya 464-8602, Japan*.

Table of Contents

Experimental details

General procedures

All the solvents were purchased from Wako Pure Chemical Industries, while the chemicals were purchased from Sigma-Aldrich Co. All the reagents were of highest quality available and were used as received. ^{1}H-NMR, and ^{31}P-NMR spectra were collected at room temperature on a JEOL JNM-ECS400 spectrometer. UV-vis absorption spectra were measured on a Shimadzu UV-2450SIM spectrophotometer at room temperature. Elemental analyses were performed on a J-Science Lab Micro Corder JM10 elemental analyzer. ESI-TOF MS spectra were collected on a JEOL JMS-T100LC mass spectrometer.

Syntheses

8-(diphenylphosphanyl)quinoline (pqn) was synthesized according to literature procedures.[S1] ^{1}H NMR ($CDCl_3$): δ 7.12 (m, 1 H), 7.30 (m, 10 H), 7.43 (m, 2 H), 7.81 (d, 1 H), 8.16 (d, 1 H), 8.87 (dd, 1 H). ^{31}P{^{1}H} NMR ($CDCl_3$): δ –14.32 (s). Anal. Found: C, 78.52; H, 5.36; N, 4.16. Calculated for $C_{21}H_{16}NP{\cdot}0.5H_2O$ (pqn·0.5 H_2O): C, 78.25; H, 5.32; N, 4.35.

trans(*P,MeCN*)-[Ru^{II}(tpy)(pqn)(MeCN)]$(PF_6)_2$ (**RuP**) was synthesized according to literature procedures.[S2] ESI-TOF MS (positive ion, acetonitrile): m/z 324.1 ([Ru(tpy)(pqn)]$^{2+}$), 344.6 ([Ru(tpy)(pqn)(MeCN)]$^{2+}$). ^{1}H NMR (CD_3CN): δ 6.56 (t, 4 H), 6.96 (t, 4 H), 7.12 (d, 2 H), 7.21 (t, 2 H), 7.55 (t, 2 H), 7.81 (t, 2 H), 7.93 (m, 3 H), 8.04 (d, 2 H), 8.21 (t, 1 H), 8.29 (d, 2 H), 8,50 (d, 1 H), 8,81 (d, 1 H), 9.83 (d, 1 H). ^{31}P{^{1}H} NMR (CD_3CN): δ 58.74 (s). Anal. Found: C, 46.02; H, 3.35; N, 7.18. Calculated for $C_{38}H_{30}N_5P_3F_{12}Ru{\cdot}0.5H_2O$ (**RuP**·0.5 H_2O): C, 46.21; H, 3.16; N, 7.09. [Ru^{II}(tpy)(bpy)(MeCN)]$(PF_6)_2$ (**RuN**) was synthesized according to literature procedures.[S3] ESI-TOF MS (positive ion, acetonitrile): m/z 266.0 ([Ru(tpy)(bpy)(MeCN)]$^{2+}$), 676.9 ([Ru(tpy)(bpy)(MeCN)]$^{+}PF_6$). ^{1}H NMR (CD_3CN): δ 7.05 (m, 1 H), 7.26 (d, 1 H), 7.32 (m, 2 H), 7.66 (d, 2 H), 7.78 (t, 1 H), 7.98 (m, 3 H), 8.30 (m, 3 H), 8.40 (d, 2 H), 8,54 (d, 2 H), 8,60 (d, 1 H), 9.58 (d, 1 H). Anal. Found: C, 39.42; H, 2.75; N, 10.24. Calculated for $C_{37}H_{22}N_6P_2F_{12}Ru$ (**RuN**): C, 39.48; H, 2.70; N, 10.23.

Electrochemistry

Electrochemical experiments were performed at room temperature on a BAS ALS Model 650DKMP electrochemical analyzer in acetonitrile or γ-butyrolactone ([cat.] = 0.5 mM; 0.1 M tetraethylammonium perchlorate (TEAP)). Cyclic voltammetry was performed by using a one-compartment cell with a three-electrode configuration, which consisted of a glassy carbon disk, platinum wire, and Ag/Ag^+ electrode (Ag/0.01 M $AgNO_3$) as the working, auxiliary, and reference electrodes, respectively. The glassy carbon disc working electrode was polished using alumina prior to each measurement. The concentration of CO_2 during the measurements was controlled using KOFLOC RK1200M and 8500MC-0-1-1 flowmeters.

UV-vis spectro-electrochemistry

A thin-layer quartz glass cell (light path length 1 mm) was used. A piece of 80 mesh platinum gauze, a platinum wire, and a Ag/Ag^+ electrode (Ag/0.01 M $AgNO_3$) were used as the working, auxiliary, and reference electrodes, respectively. All solutions were purged with Ar or saturated with CO_2 (0.28 M) before the measurements. Spectra were obtained after electrolysis at appropriate potentials for 8 mins. UV-vis spectra in the range from 250−800 nm were recorded. The temperature was controlled at 20 ˚C during the measurements, and a weak Ar/CO_2 flow was supplied throughout the experiments. The redox potentials of samples were calibrated against the redox signal for the ferrocene/ferrocenium (Fc/Fc^+) couple.

Controlled-potential electrolysis

Controlled-potential electrolysis was performed in a gas-tight two-compartment electrochemical cell. In the first compartment, the carbon rod working electrode (1.2 cm^2 surface area) and a leakless Ag/AgCl reference electrode (Innovative Instruments, Inc.) were immersed in 0.1 M TEAP/MeCN (5 ml) containing the catalyst (0.5 mM) and H_2O (2.65 M). In the second compartment, the Pt auxiliary electrode was immersed in 0.1 M TEAP/MeCN (5 ml) containing ferrocene (40 mM) as a sacrificial reductant. The two compartments were separated by an anion exchange membrane (Selemion DSV). The solution was purged vigorously with CO_2 for 30 min prior to electrolysis. The electrolysis was performed for 1 h with constant stirring. The amount of CO and H_2 produced at the headspace of the cell was

quantified by a Shimadzu GC-8A with a TCD detector equipped with a packed column with Molecular Sieve 13X-S 60/80. Additionally, liquid product was quantified by using a Shimadzu LC-20AD with SPD-20A and RID-10A detectors equipped with a Shim-pack SCR102H column. Calibration curves were obtained by sampling known amounts of H_2, CO, and HCOOH.

DFT calculations

Geometric optimization and electronic structures were obtained at the B3LYP or UB3LYP functional[S4,S5] and LanL2DZ basis set[S6,S7] with the Gaussian 09 program package.[S8]

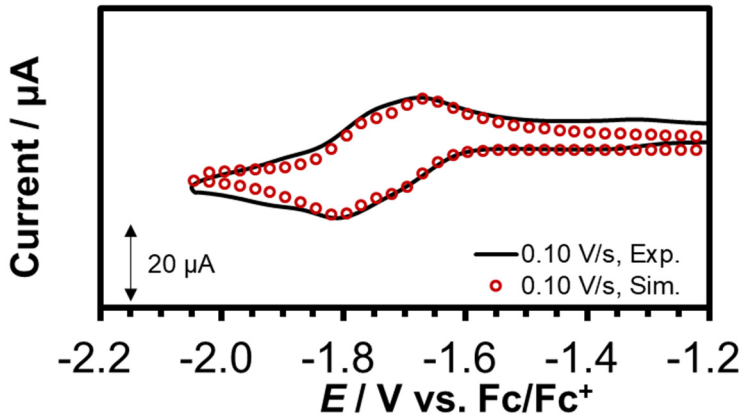

Figure S1. A CV of **RuP** in acetonitrile (black line, [complex] = 0.5 mM; 0.1 M TEAP; WE: GC, CE: Pt wire, RE: Ag/Ag^{+}, scan rate, 0.10 V/s) under Ar, and the simulated CV (red circle). Elchsoft DigiElch 7.FD software was used for simulation of CV to obtain redox potentials of **RuP** as reported previously.[S2]

Table S1. Simulation parameters for the CV. Elchsoft DigiElch 7.0. software was used for simulation.

	RuP
Sweep rate [*v*] (V/s)	0.10
Resistance [*R*] (Ω)	200
Capacitance [*CdI*] (F)	7.0×10^{-6}
Temperature [*T*] (K)	293
Surface area [*A*] (cm^2)	0.07
Diffusion constant [*D*] (cm^2/s)	1.0×10^{-5}
Concentration [*c*] (mol/dm^3)	5.0×10^{-4}
$E\,°'_1$ (V)	−1.69
k_{s1} (cm/s)	0.05
α_1	0.50
$E\,°'_2$ (V)	−1.78
k_{s2} (cm/s)	0.05
α_2	0.50

$E\,°'_1$ and $E\,°'_2$ are referred to Fc/Fc^+.

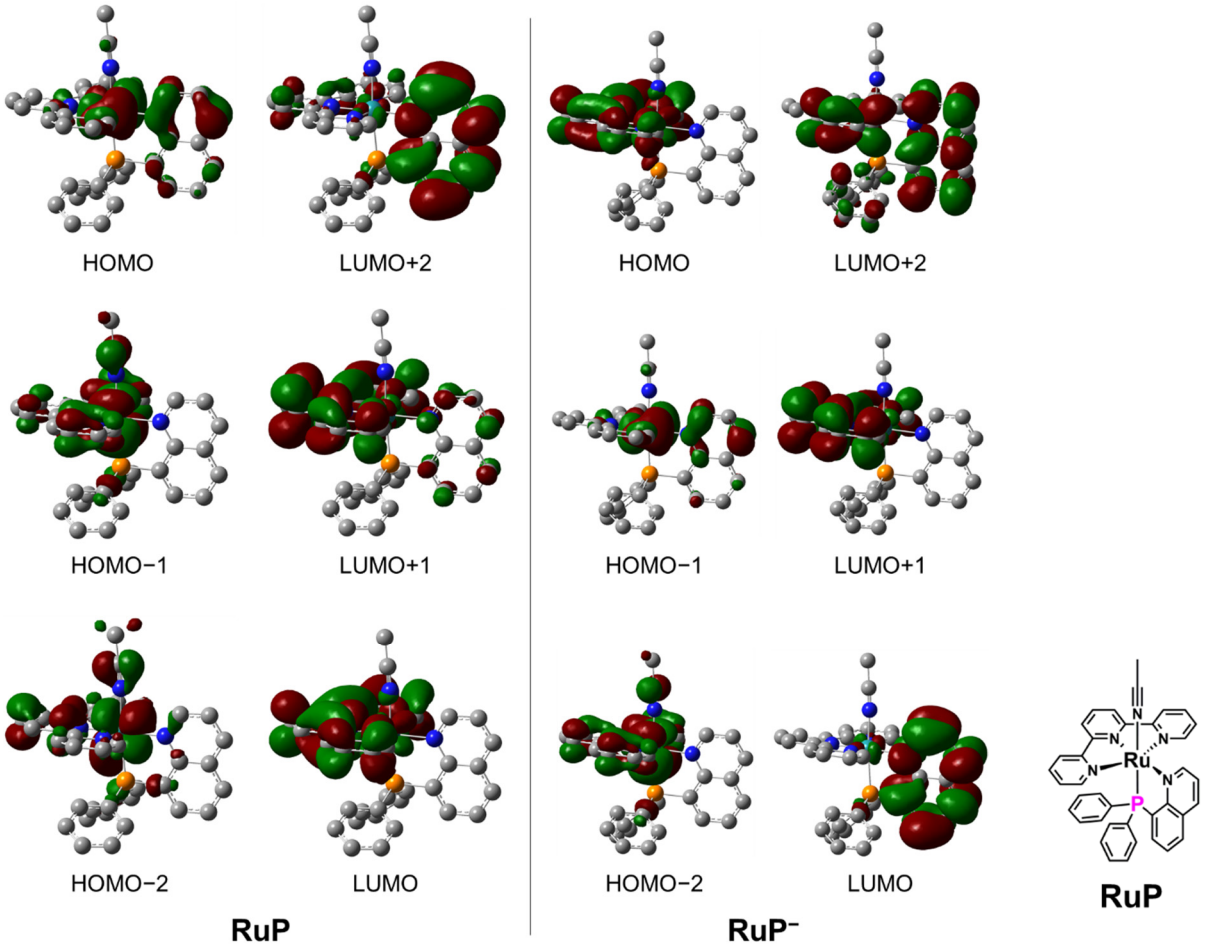

Figure S2. Isodensity surface plots of selected frontier molecular orbitals of **RuP** and **RuP**$^{-}$ based on the optimized ground-state geometry. The geometric optimization and electronic structures for **RuP** and **RuP**$^{-}$ were calculated at the B3LYP/LanL2DZ level and UB3LYP/LanL2DZ level, respectively with the Gaussian 09 program package.

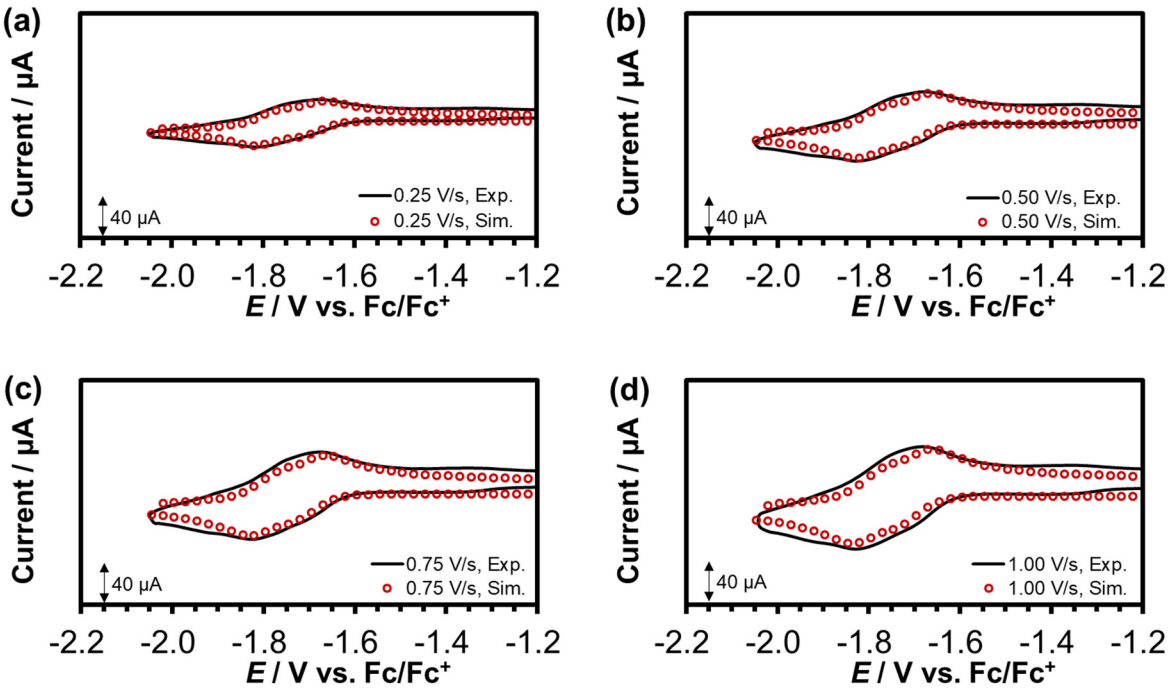

Figure S3. Experimental (black lines) and simulated CVs (red circles) of **RuP** (0.5 mM) in 0.1 M TEAP/MeCN under Ar at various scan rates, (a) = 0.25 V/s, (b) = 0.50 V/s, (c) = 0.75 V/s, (d) = 1.00 V/s. Working electrode, glassy carbon; counter electrode, Pt wire; reference electrode, Ag/Ag^{+}.

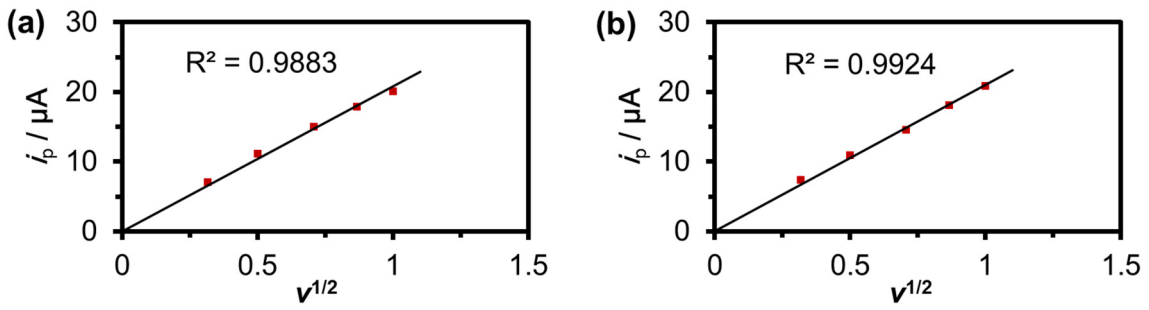

Figure S4. Variation of peak current (i_p) of **RuP** (0.5mM) at the (a) first redox wave and (b) second redox wave versus square root of scan rate. The i_p values were obtained from simulated CVs.

Table S2. Summary of the data used for the i_p vs. $v^{1/2}$ plot.

		First redox wave	Second redox wave
v (V/s)	$v^{1/2}$	i_p (µA)	i_p (µA)
0.10	0.316	7.00	7.41
0.25	0.500	11.13	10.95
0.50	0.707	15.06	14.60
0.75	0.866	17.89	18.05
1.00	1.00	20.13	20.90

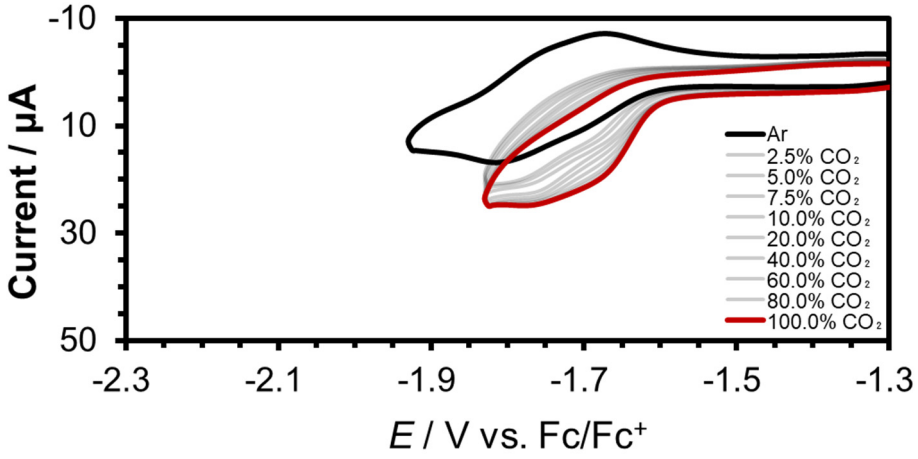

Figure S5. CVs of **RuP** (0.5 mM) in anhydrous 0.1 M TEAP/MeCN under various concentrations of CO_2 (CO_2/Ar, v/v%). Working electrode, glassy carbon; counter electrode, Pt wire; reference electrode, Ag/Ag^+; scan rate, 0.1 V/s.

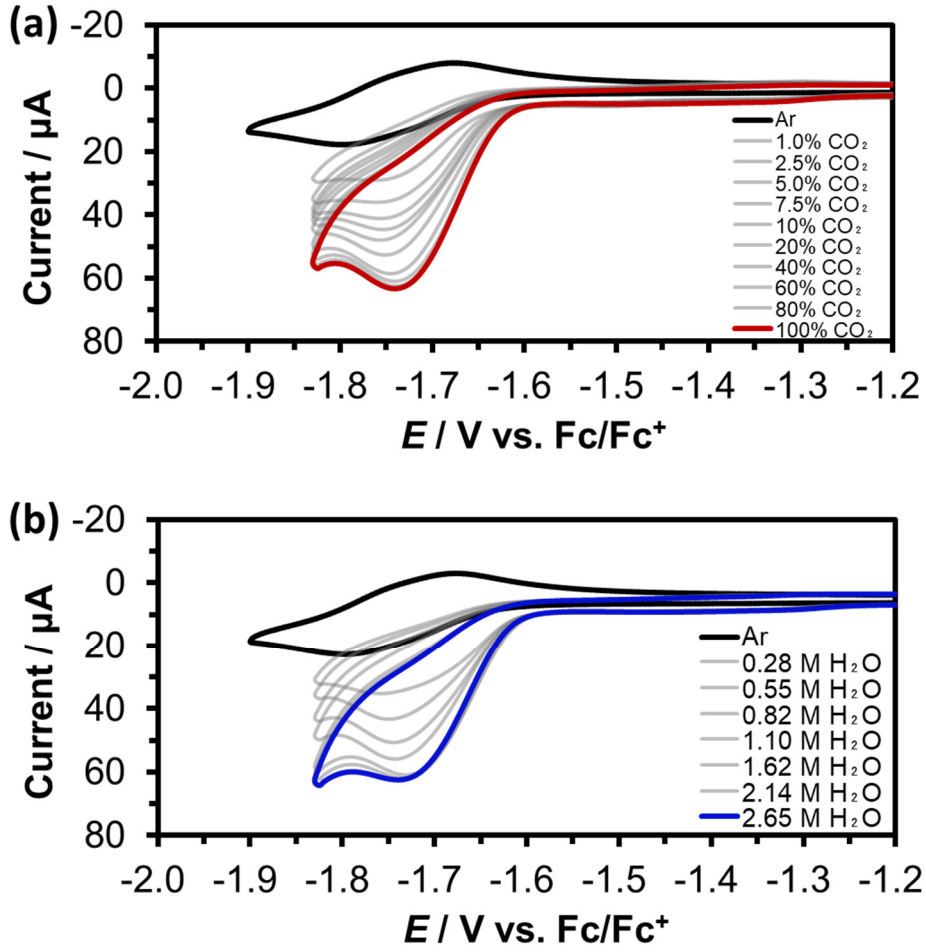

Figure S6. (**a**) CVs of **RuP** (0.5 mM) in 0.1 M TEAP/MeCN under various concentrations of CO_2 (CO_2/Ar, v/v%) in the presence of H_2O (2.65 M). (**b**) CVs of **RuP** (0.5 mM) in 0.1 M TEAP/MeCN at various concentrations of H_2O under CO_2 (0.28 M). Working electrode, glassy carbon; counter electrode, Pt wire; reference electrode, Ag/Ag^+; scan rate, 0.1 V/s.

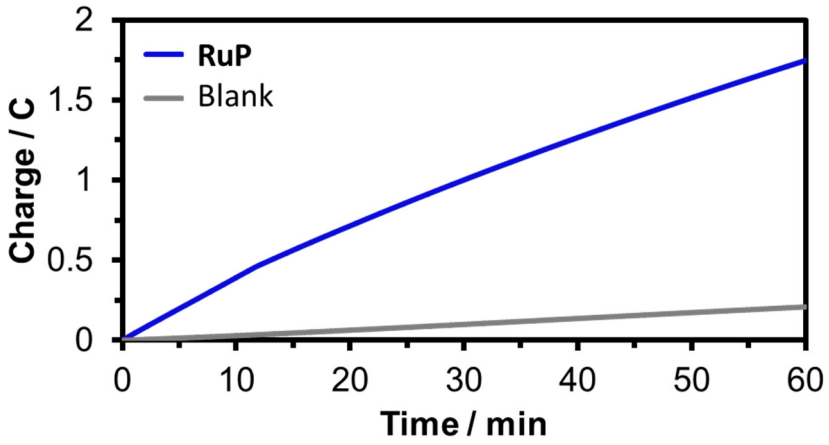

Figure S7. The result of controlled-potential electrolysis of **RuP** (0.5 mM) in 0.1 M TEAP/MeCN under CO_2 (0.28 M) at −1.7 V (vs. Fc/Fc^+) in the presence of H_2O (2.65 M) for 1 h. Working electrode, glassy carbon (1.2 cm^2); counter electrode, Pt wire; reference electrode, Ag/AgCl. Approximately 1.75 C has been transferred during 1 h of electrolysis.

Table S3. Summary of CPE experiments[a]

Entry	Catalyst	[H_2O], M	Charge, C	Faradaic Efficiency, %[b]		
				CO	HCOOH	H_2
1	**RuP**	2.65	1.75	55.8	6.6	0.5
2	-	2.65	0.15	-	-	-

[a] Conditions: 0.50 mM catalyst, applied voltage: −1.70 V (vs. Fc/Fc^+), duration: 1 h.

[b] Further reduced species of CO_2 such as formaldehyde and methanol have not been detected, and the fate of the rest of the charge is not clear at this stage.

Table S4. Overpotentials (η) and operating conditions of selected homogeneous CO_2 reduction electrocatalysts

Entry Molecule	Solvent	Overpotentials, η (V)	TOF (s^{-1})	Ref.
$[Ru(tpy)(pqn)(MeCN)]^{2+}$ (**RuP**)	MeCN + 2.65 M H_2O	0.40[a,b]	4.7[f]	This work
$[Ru(tpy)(bpy)(MeCN)]^{2+}$ (**RuN**)	MeCN + 2.65 M H_2O	0.60[a,b]	5.1[e]	S9
	MeCN	0.87	5.5[e], 38.4[f]	S10, S11
$[Ru(tpy)(Mebim\text{-}py)(MeCN)]^{2+}$	MeCN	0.81	19[e], 31[f]	S10, S11
$[Ru(tpy)(bpy)(CO)]^{2+}$	MeCN	0.50[a, c]	-	S12
$[Ru(t\text{Bu}_3tpy)(6\text{-}mbpy)(MeCN)]^{2+}$	MeCN	0.47	1.1[e]	S13
trans(Cl)-$Ru(mesbpy)(CO)_2Cl_2$	MeCN + 0.5 M phenol	0.75 [a,c]	1300[g]	S14
$[Mn(mesbpy)(CO)_3(MeCN)](OTf)$	MeCN + 3.2 M MeOH	0.70	2000[g]	S15
	MeCN + 120 mM Mg^{2+}	0.30−0.45[d]	20[g]	S16
FeTDHPP	DMF + 2 M H_2O	0.41−0.56	3200[f]	S11
Fe-*o*-TMA	DMF + 3 M phenol	0.22	100000[f]	S17

[a]The overpotentials, η, were calculated using previously reported methods,[S18] which is the difference between the standard potential of CO_2/CO couple in a specific solvent system with potential at half the catalytic current ($E_{cat/2}$) of catalyst (Eq. S1).

$$\eta = |E_{CO_2/CO} - E_{cat/2}| \quad \text{(Eq. S1)}$$

[b]Calculated based on the data shown in Figure S11.

[c]The values of $E_{cat/2}$ were estimated from the CVs reported in the references.

For the standard potential of CO_2/CO couple, $E°_{CO_2/CO,\ MeCN}$ = −1.25 V vs. Fc/Fc^+ or $E°_{CO_2/CO,\ DMF}$ = −1.30 V vs. Fc/Fc^+ was used.[S11]

[d]$E°_{CO_2}$ for $2CO_2 + Mg^{2+} \rightarrow CO + MgCO_3$ was estimated between −1.15 V to −1.30 V vs. Fc/Fc^+.[S16]

[e]The value is calculated based on results of CV as reported in S10.

[f]The value is calculated based on results of controlled potential electrolysis as reported in S11.

[g]The value is calculated based on results of CV as reported in S15.

Estimation of TOF and TON for **RuP** from controlled-potential electrolysis

$$\frac{i}{FA} = \frac{\sqrt{k_{\mathrm{cat}}D}[\mathrm{cat}]}{1+\exp\left[\frac{F}{RT}\left(E_{\mathrm{applied}}-E^{\circ}_{\mathrm{cat}}\right)\right]} \qquad \text{(Eq. S2)}$$

$$\mathrm{TOF} = \frac{k_{\mathrm{cat}}}{(1+\exp\left[\frac{F}{RT}\left(E_{\mathrm{applied}}-E^{\circ}_{\mathrm{cat}}\right)\right]} \qquad \text{(Eq. S3)}$$

$$\mathrm{TON} = \frac{k_{\mathrm{cat}}t}{(1+\exp\left[\frac{F}{RT}\left(E_{\mathrm{applied}}-E^{\circ}_{\mathrm{cat}}\right)\right]} \qquad \text{(Eq. S4)}$$

The equations were previously adapted by Savéant *et al*. in electrocatalytic CO_2 reduction reaction.[S11] By using these formula, the amount of active catalyst is the number of moles contained within the thin reaction-diffusion layer that develops adjacent to the electrode surface.[S11] In these equations, *i* represents stable current transferred during controlled-potential electrolysis, *F* is Faraday constant (96485 C/mol), *A* is the surface area of working electrode (1.2 cm^2), k_{cat} is the overall rate constant of the catalytic CO_2 reduction reaction, *D* is the diffusion coefficient (~5 x 10^{-6} cm^2/s), [cat] is the concentration of catalyst used (5 x 10^{-7} mol/cm^3), *R* is the universal gas constant (8.31 J K^{-1} mol^{-1}), *T* is temperature (298 K), $E_{applied}$ is the applied potential during electrolysis, $E°_{cat}$ is the standard potential of the catalyst, *t* is the electrolysis duration, TOF is the turnover frequency, and TON is the turnover number.

The average current density of 0.42 mA/cm^2 (the faradaic efficiency for CO formation is 56 %, corresponds to i/A = 0.24 mA/cm^2) was obtained for 1 h electrolysis at –1.70 V vs. Fc/Fc^+. Since the electrolysis is performed on the plateau of the catalytic wave, $i/FA = (k_{cat}D)^{1/2}[cat]$ (Eq. S2) leading to the TOF = 4.7 s^{-1} and TON = 1.7 x10^4. We also calculated the TON value based on the total cell volume and the value was estimated to be 2 for 1h. The result indicate the CO_2 reduction reaction mediated by **RuP** is catalytic.

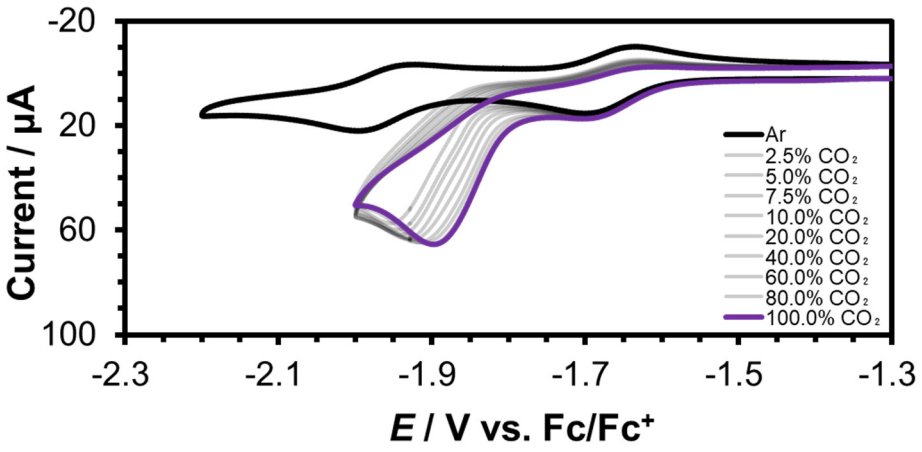

Figure S8. CVs of **RuN** (0.5 mM, open circuit = −0.27 V) in 0.1 M TEAP/MeCN under various concentrations of CO_2 (CO_2/Ar, v/v%) in the absence of H_2O. Working electrode, glassy carbon; counter electrode, Pt wire; reference electrode, Ag/Ag^+; scan rate, 0.1 V/s.

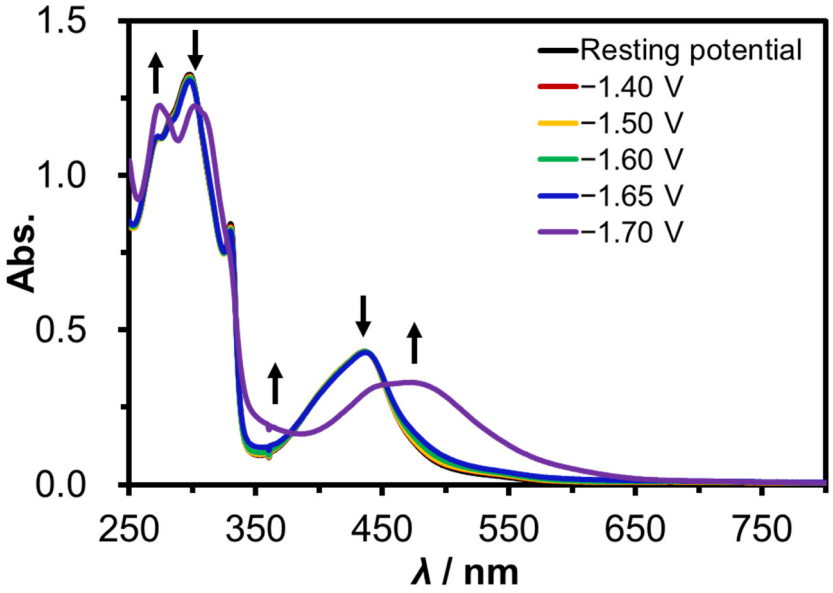

Figure S9. Experimental UV-Vis absorption spectra of **RuP** (0.5 mM) at various applied potentials in 0.1 M TEAP/MeCN under Ar using BASi Spectro-electrochemical Cell (open-circuit potential = −0.27 V). Working electrode, Pt mesh; counter electrode, Pt wire; reference electrode, Ag/Ag^{+}. Solutions were purged with Ar for 10 mins prior to measurements. Weak Ar flow was maintained throughout the measurement. Spectra were acquired after electrolysis at respective potentials for 8 mins.

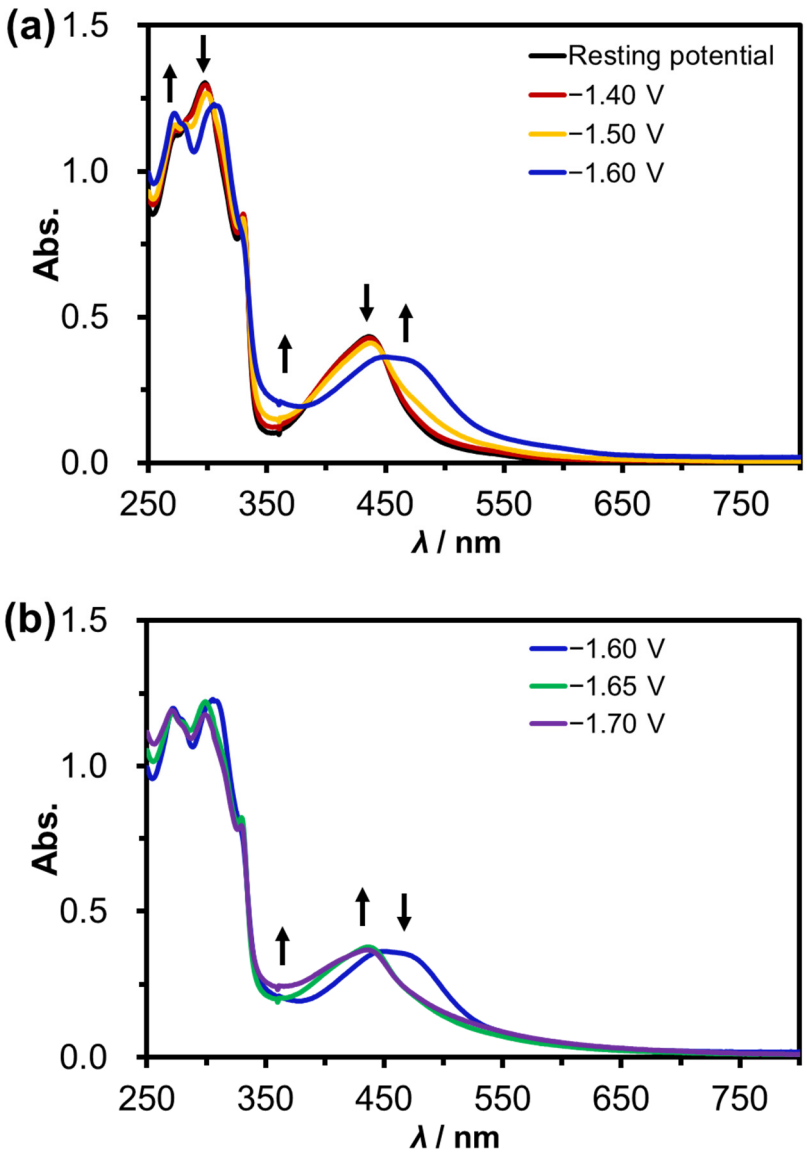

Figure S10. Experimental UV-Vis absorption spectra of **RuP** (0.5 mM) at various applied potentials in 0.1 M TEAP/MeCN under CO_2. (a) Resting potential to −1.60 V and (b) −1.60 V to −1.70 V. Working electrode, Pt mesh; counter electrode, Pt wire; reference electrode, Ag/Ag^+. Spectra were acquired after electrolysis at respective potentials for 8 mins.

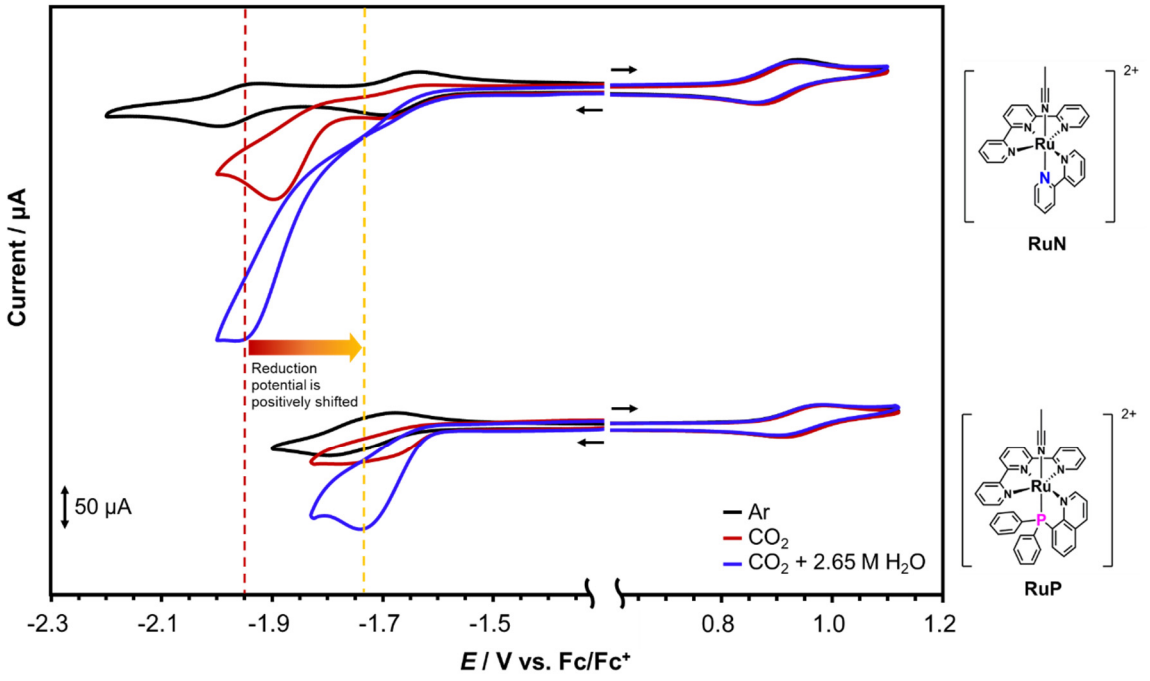

Figure S11. CVs of 0.5 mM of **RuN** (top) and **RuP** (bottom) in 0.1 M TEAP/MeCN under Ar (black line), CO_2 (0.28 M, red line), and CO_2 in the presence of 2.65 M H_2O (blue line). Working electrode, glassy carbon; counter electrode, Pt wire; reference electrode, Ag/Ag^+; scan rate, 0.1 V/s. Potential sweeps were started from the open circuit potential (−0.26 V for **RuN**, −0.27 V for **RuP**). Arrows represent the direction of potential sweeping. In the presence of H_2O, the current enhancement was observed at E_{pc} = −1.95 V for **RuN** and E_{pc} = −1.73 V for **RuP**, which attributed to the electrocatalytic CO_2 reduction.

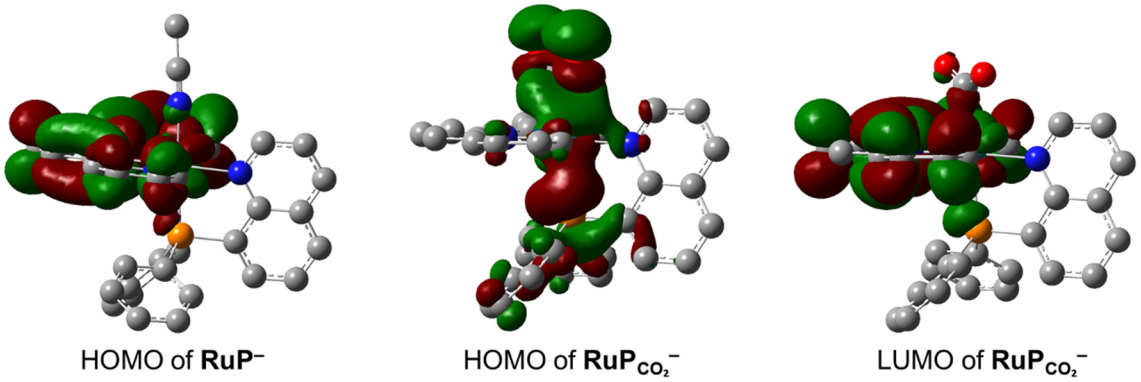

Figure S12. HOMO of the one-electron reduced species, **RuP**$^{-}$ (left) and HOMO–LUMO of one-electron reduced **RuP** with a CO_2 molecule bound to the Ru center, **RuP**$_{CO_2}^{-}$ (middle & right) based on the optimized ground-state geometry. DFT calculations were performed using the UB3LYP functional and LanL2DZ basis set.

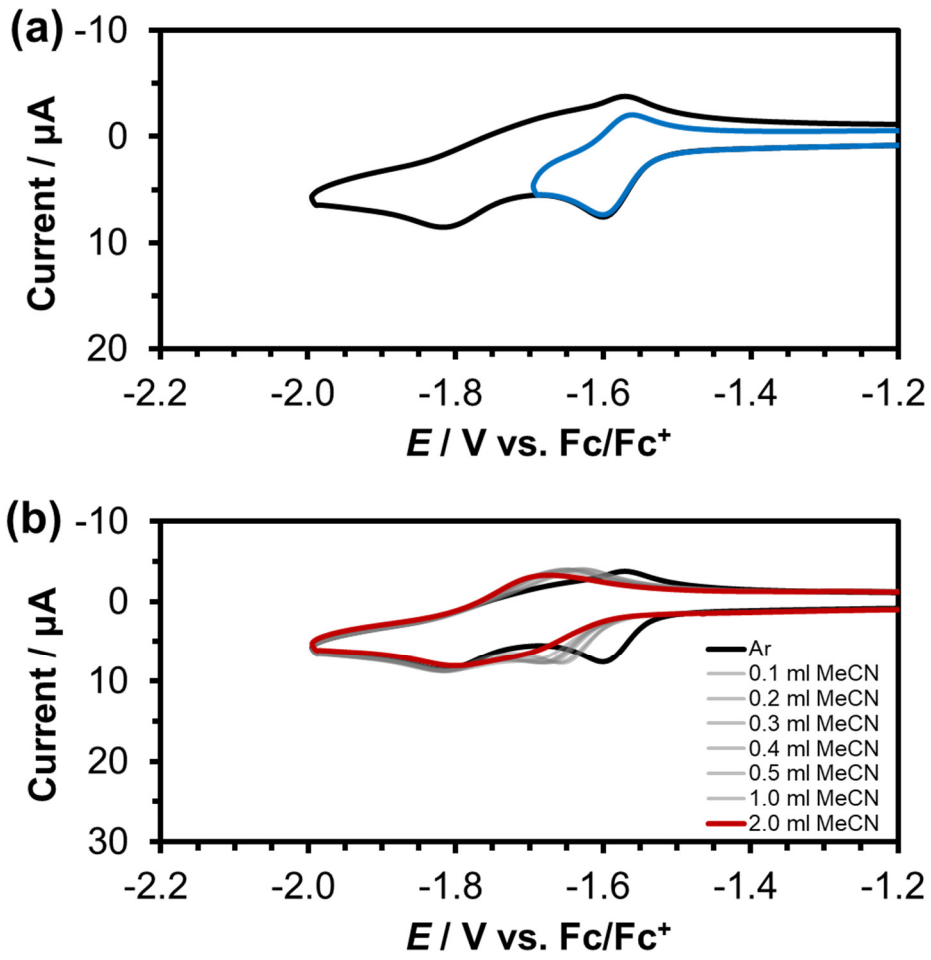

Figure S13. (a) CV of **RuP** (0.5 mM) in 0.1 M TEAP/γ-butyrolactone under Ar at different potential scan range. (b) CV of **RuP** (0.5 mM) in 0.1 M TEAP/γ-butyrolactone under Ar added with various amount of MeCN. Working electrode, glassy carbon; counter electrode, Pt wire; reference electrode, Ag/Ag^+; scan rate, 0.1 V/s.

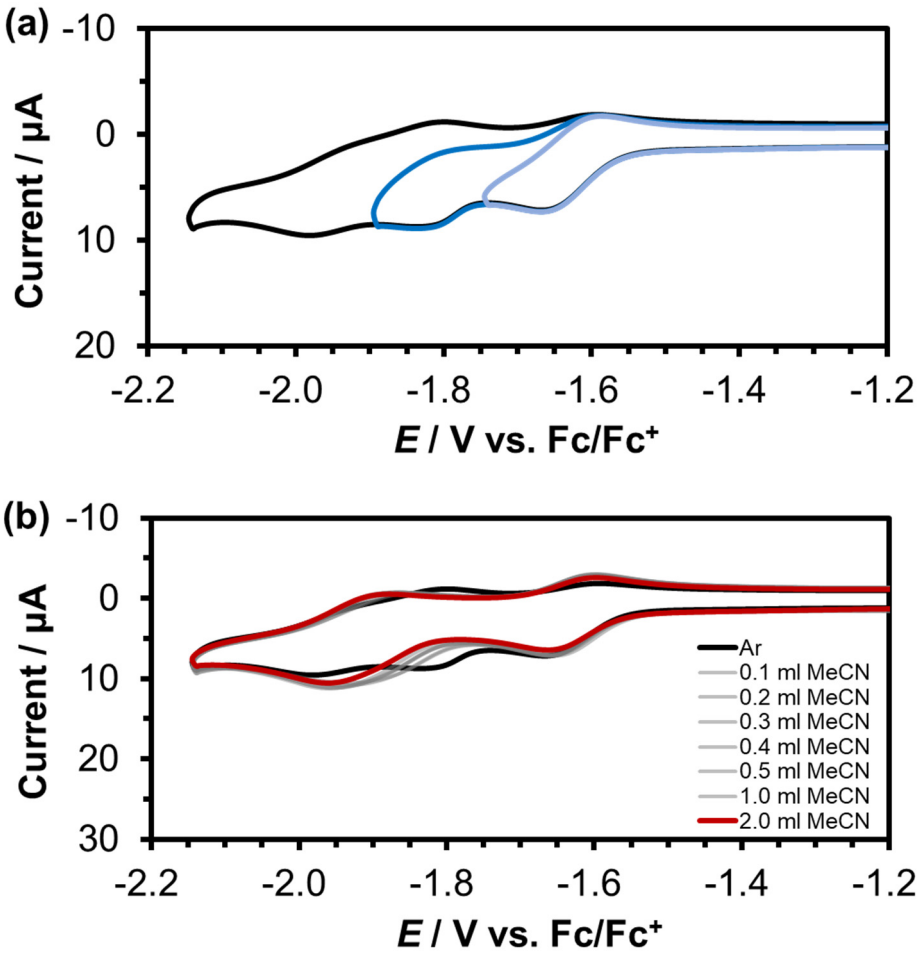

Figure S14. (a) CV of **RuN** (0.5 mM) in 0.1 M TEAP/γ-butyrolactone under Ar at different potential scan range. (b) CV of **RuN** (0.5 mM) in 0.1 M TEAP/γ-butyrolactone under Ar added with various amount of MeCN. Working electrode, glassy carbon; counter electrode, Pt wire; reference electrode, Ag/Ag^+; scan rate, 0.1 V/s.

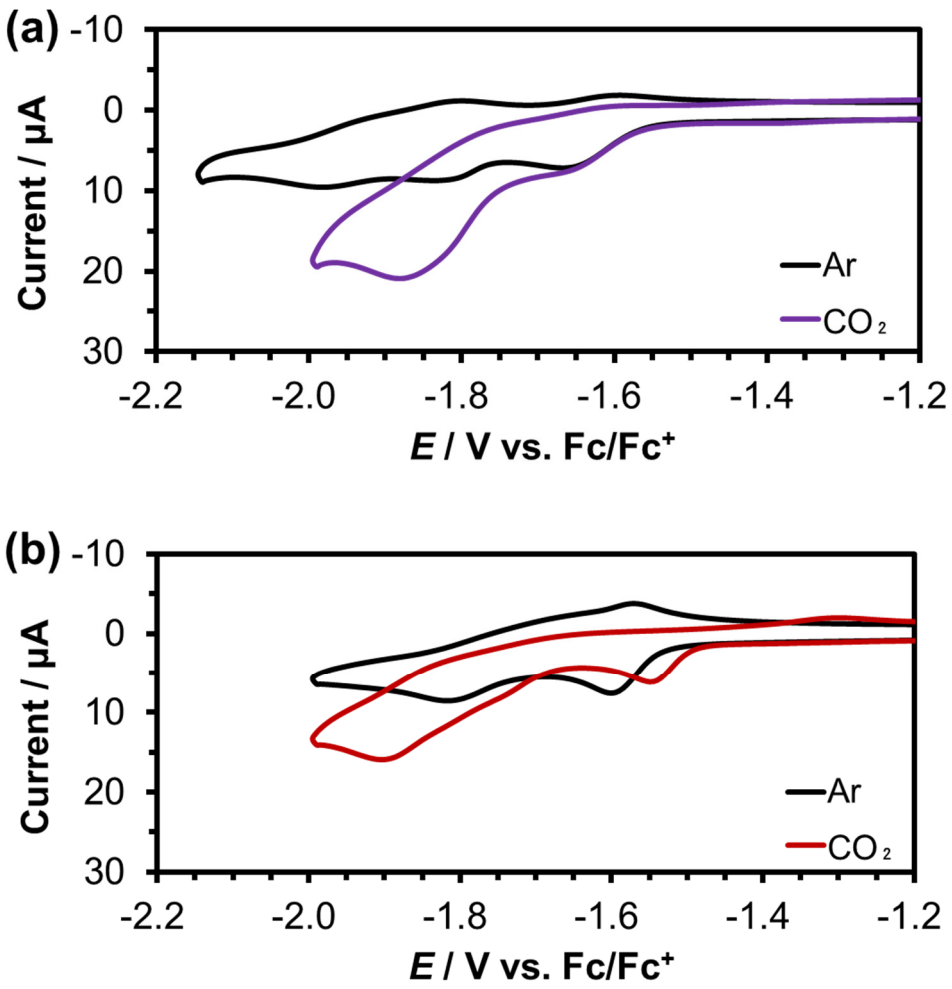

Figure S15. (a) CVs of **RuN** (0.5mM) in 0.1 M TEAP/γ-butyrolactone under CO_2. (b) CVs of **RuP** (0.5 mM) in 0.1 M TEAP/γ-butyrolactone under CO_2. Working electrode, glassy carbon; counter electrode, Pt wire; reference electrode, Ag/Ag^+; scan rate, 0.1 V/s.

References

S1 T. Suzuki, T. Kuchiyama, S. Kishi, H. D. Takagi, M. Kato, *Inorg. Chem.* 2003, **42**, 785.

S2 G. Nakamura, M. Okamura, M. Yoshida, T. Suzuki, H. D. Takagi, M. Kondo, S. Masaoka, *Inorg. Chem.* 2014, **53**, 7214.

S3 K. J. Takeuchi, M. S. Thompson, D. W. Pipes, T. J. Meyer, *Inorg. Chem*. 1984, **23**, 1845.

S4 C. Lee, W. Yang, R. G. Parr, *Phys. Rev. B* 1988, **37**, 785.

S5 A. D. Becke, *J. Chem. Phys.* 1993, **98**, 5648.

S6 P. J. Hay, W. R. Wadt, *J. Chem. Phys.* 1985, **82**, 299.

S7 P. J. Hay, W. R. Wadt, *J. Chem. Phys.* 1985, **82**, 270.

S8 M. J. Frisch, G. W. Trucks, H. B. Schlegel, G. E. Scuseria, M. A. Robb, J. R. Cheeseman, G. Scalmani, V. Barone, B. Mennucci, G. A. Petersson, H. Nakatsuji, M. Caricato, X. Li, H. P. Hratchian, A. F. Izmaylov, J. Bloino, G. Zheng, J. L. Sonnenberg, M. Hada, M. Ehara, K. Toyota, R. Fukuda, J. Hasegawa, M. Ishida, T. Nakajima, Y. Honda, O. Kitao, H. Nakai, T. Vreven, J. A. Jr. Montgomery, J. E. Peralta, F. Ogliaro, M. Bearpark, J. J. Heyd, E. Brothers, K. N. Kudin, V. N. Staroverov, T. Keith, R. Kobayashi, J. Normand, K. Raghavachari, A. Rendell, J. C. Burant, S. S. Iyengar, J. Tomasi, M. Cossi, N. Rega, J. M. Millam, M. Klene, J. E. Knox, J. B. Cross, V. Bakken, C. Adamo, J. Jaramillo, R. Gomperts, R. E. Stratmann, O. Yazyev, A. J. Austin, R. Cammi, C. Pomelli, J. W. Ochterski, R. L. Martin, K. Morokuma, V. G. Zakrzewski, G. A. Voth, P. Salvador, J. J. Dannenberg, S. Dapprich, A. D. Daniels, O. Farkas, J. B. Foresman, J. V. Ortiz, J. Cioslowski, D. J. Fox, *Gaussian 09 (Revision C.01)*, Gaussian, Inc., Wallingford, CT, 2010.

S9 Z. Chen, P. Kang, M. T. Zhang, T. J. Meyer, *Chem. Commun*. 2014, **50**, 335.

S10 Z. Chen, C. Chen, D. R. Weinberg, P. Kang, J. J. Concepcion, D. P. Harrison, M. S. Brookhart, T. J. Meyer, *Chem. Commun.* 2011, **47**, 12607.

S11 C. Costentin, S. Drouet, M. Robert, J. M. Savéant, *Science* 2012, **338**, 90.

S12 H. Nagao, T. Mizukawa, K. Tanaka, *Inorg. Chem.* 1994, **33**, 3415.

S13 B. A. Johnson, S. Maji, H. Agarwala, T. A. White, E. Mijangos, S. Ott, *Angew. Chem. Int. Ed.* 2016, **55**, 1825.

S14 C. W. Machan, M. D. Sampson, C. P. Kubiak, *J. Am. Chem. Soc.* 2015, **137**, 8564.

S15 M. D. Sampson, A. D. Nguyen, K. A. Grice, C. E. Moore, A. L. Rheingold, C. P. Kubiak, *J. Am. Chem. Soc.* 2014, **136**, 5460.

S16 M. D. Sampson, C. P. Kubiak, *J. Am. Chem. Soc.* 2016, **138**, 1386.

S17 I. Azcarate, C. Costentin, M. Robert, J. M. Savéant, *J. Am. Chem. Soc*. 2016, **138**, 16639.

S18 A. M. Appel, M. L. Helm, *ACS Catal*. 2014, **4**, 630.